Remote Sensing Imagery and Signature Fields Reconstruction via Aggregation of Robust Regularization With Neural Computing

Yuriy Shkvarko[1], and Ivan Villalon-Turrubiates[1]

[1] CINVESTAV Jalisco, Avenida Científica 1145, Colonia El Bajío, 45010,
Telephone (+52 33) 3770-3700, Fax (+52 33) 3770-3709, Zapopan Jalisco, México
{shkvarko, villalon}@gdl.cinvestav.mx
http://www.gdl.cinvestav.mx

Abstract. The robust numerical technique for high-resolution reconstructive imaging and scene analysis is developed as required for enhanced remote sensing with large scale sensor array radar/synthetic aperture radar. First, the problem-oriented modification of the previously proposed fused Bayesian-regularization (FBR) enhanced radar imaging method is performed to enable it to reconstruct remote sensing signatures (RSS) of interest alleviating problem ill-poseness due to system-level and model-level uncertainties. Second, the modification of the Hopfield-type maximum entropy neural network (NN) is proposed that enables such NN to perform numerically the robust adaptive FBR technique via efficient NN computing. Finally, we report some simulation results of hydrological RSS reconstruction from enhanced real-world environmental images indicative of the efficiency of the developed method.

1 Introduction

Modern applied theory of reconstructive image processing is now a mature and well developed research field, presented and detailed in many works (see, for example [1] thru [16] and references therein). Although the existing theory offers a manifold of statistical and descriptive regularization techniques for reconstructive imaging in many application areas there still remain some unresolved crucial theoretical and processing problems related to large scale sensor array real-time reconstructive image processing.

In this study, we consider the problem of enhanced remote sensing (RS) imaging and reconstruction of remote sensing signature (RSS) fields of the RS scenes with the use of array radars or synthetic aperture radars (SAR) as sensor systems. Two principal algorithmic-level and computational-level developments constitute major innovative contributions of this study, namely:

1) Development of a robust version of the fused Bayesian-regularization (FBR) method [1], [5] for reconstruction of the power spatial spectrum pattern (SSP) of the wave field scattered from the RS scene [7] and related RSS given a finite set of SAR signal recordings. Since this is in essence a nonlinear numerical inverse problem, we propose to alleviate the problem ill-poseness via robustification of the Bayesian estimation strategy [6], [7] by performing the non adaptive approximations of the SSP and RSS reconstructive operators that incorporate the non trivial metrics considerations for designing the proper solution space and different regularization constraints imposed on a solution.

2) Design of numerical techniques for efficient real-time computational implementation of the robust RS image enhancement and RSS field reconstruction algorithms that employ the neural network (NN) computing. In particular, we propose to employ the general Li's architecture of the Hopfield-type dynamic NN detailed in [5] and [8] but modify the specifications of the NN's parameters (i.e. synaptic weights and bias inputs in all the NN's loops, as well as the NN's state update rule) to enable such the modified NN to perform the real-time robust image enhancement and RSS field reconstruction tasks. Also, we propose a method to perform such a reconstruction with controllable balance between the achievable spatial resolution and admissible noise level in the resulting image/RSS map.

2 Problem Model

Consider the measurement data wavefield $u(\mathbf{y})=s(\mathbf{y})+n(\mathbf{y})$ modeled as a superposition of the echo signals s and additive noise n that assumed to be available for observations and recordings within the prescribed time-space observation domain $Y \ni \mathbf{y}$, where $\mathbf{y}=(t,\mathbf{p})^{\mathrm{T}}$ defines the time-space points in the observation domain $Y=T\cdot P$. The model of observation wavefield u is specified by the linear stochastic equation of observation (EO) of operator form [5]: $u=Se+n$; $e \in \mathrm{E}$; $u,n \in \mathrm{U}$; $S:\mathrm{E}\to\mathrm{U}$, in the L_2 Hilbert signal spaces E and U with the metric structures induced by inner products,

$$[e_1,e_2]_{\mathrm{E}}=\int_{F\times X} e_1(f,\mathbf{x})e_2^{*}(f,\mathbf{x})dfd\mathbf{x}\,,\quad [u_1,u_2]_{\mathrm{U}}=\int_{Y} u_1(\mathbf{y})u_2^{*}(\mathbf{y})d\mathbf{y}\,, \tag{1}$$

respectively. The operator model of the stochastic EO in the conventional integral form may be rewritten as [1]

$$u(\mathbf{y})=\int_{F\times X} S(\mathbf{y},\mathbf{x})e(f,\mathbf{x})dfd\mathbf{x}+n(\mathbf{y})\,, \tag{2}$$

$$e(f,\mathbf{x})=\int_{T} \varepsilon(t;\mathbf{x})\exp(-j2\pi ft)dt \tag{3}$$

where $\varepsilon(t;\mathbf{x})$ represents the stochastic backscattered wavefield fluctuating in time t, and the functional kernel $S(\mathbf{y},\mathbf{x})$ of the signal formation operator (SFO) S in (2) is specified by the particular employed RS signal wavefield formation model [1]. The phasor $e(f,\mathbf{x})$ in (1), (2) represents the backscattered wavefield $e(f,\boldsymbol{\rho},\boldsymbol{\theta})$ over the frequency-space observation domain $F\cdot P\cdot\Theta$; in the slant range $\boldsymbol{\rho}\in P$ and azimuth angle $\boldsymbol{\theta}\in\Theta$ domains, respectively. When considering the RS spectral analysis problems, the radar engineers typically work in the frequency-space domain, $(f;\boldsymbol{\rho},\boldsymbol{\theta})^{\mathrm{T}}\in F\cdot P\cdot\Theta$, however, because of the one-to-one mapping [4], [9] only the spatial cross range coordinates $(\boldsymbol{\rho},\boldsymbol{\theta})^{\mathrm{T}}$ are usually associated with the RS scene [9], i.e. $\mathbf{x}=(\boldsymbol{\rho},\boldsymbol{\theta})^{\mathrm{T}}\in X=P\cdot\Theta$. This is valid for any narrowband RS system model [13] and incoherent nature of the backscattered wavefield $e(f,\mathbf{x})$ that is naturally inherent to the RS imaging experiments [4], [9], [13]. Following such model assumptions, the phasor $e(f,\mathbf{x})$ in (2), (3) is taken to be an independent random variable at each frequency f, and spatial coordinates $\mathbf{x}$ with the zero mean value and δ-form correlation function, $R_e(f,f';\mathbf{x},\mathbf{x}')=\langle e(f,\mathbf{x})e^{*}(f',\mathbf{x}')\rangle=b(f,\mathbf{x})\delta(f-f')\delta(\mathbf{x}-\mathbf{x}')$ that enables one to introduce the following definition of the spatial spectrum pattern (SSP)

$$B(\mathbf{x})=Aver^{(2)}\{e(\mathbf{x})\}=\int_{F}\left\langle e(f,\mathbf{x})e^{*}(f,\mathbf{x})\right\rangle |H(f)|^{2}df\,;\quad \mathbf{x}\in X\,. \tag{4}$$

Here, $\langle\cdot\rangle$ represents the ensemble averaging operator, while $Aver^{(2)}$ is referred to as the second order statistical averaging operator defined by (4), $H(f)$ represents the given transfer function of the radar receiving channels that we assume to be identical for all antenna array elements and impose the conventional normalization, $|H(f)|^{2}=1$ for all frequencies $f\in F$ in the radar receiver frequency integrating band F. The RS imaging problem is stated as follows: to find an estimate $\hat{B}(\mathbf{x})$ of the SSP $B(\mathbf{x})$ in the environment $X\ni\mathbf{x}$ by processing whatever values of measurements of the data wavefield $u(\mathbf{y})$; $\mathbf{y}\in Y$, are available. Following the RS methodology [5], any particular physical RSS of interest is to be extracted from the reconstructed RS image $\hat{B}(\mathbf{x})$ applying the so-called signature extraction operator Λ. Hence, the particular RSS is mapped applying Λ to the reconstructed image, i.e.

$$\hat{\Lambda}(\mathbf{x})=\Lambda(\hat{B}(\mathbf{x}))\,. \tag{5}$$

Last, taking into account the RSS extraction model (5), we can reformulate now the signature reconstruction problem as follows: to map the reconstructed particular RSS of interest $\hat{\Lambda}(\mathbf{x})=\Lambda(\hat{B}(\mathbf{x}))$ over the observation scene $X\ni\mathbf{x}$ via post-processing (5) whatever values of the reconstructed scene image $\hat{B}(\mathbf{x})$; $\mathbf{x}\in X$ are available. For an RS system with an arbitrary sensor configuration, the recorded data is traditionally expressed as a discrete-form version of the EO (1)

$$\mathbf{U}=\mathbf{SE}+\mathbf{N} \tag{6}$$

where **E**, **N** and **U** define the zero-mean vectors composed of the coefficients E_k, N_m, and U_m of the numerical approximations of the relevant operator-form EO (1), i.e. **E** represents the K-D vector composed with the coefficients $\{E_k=[e,g_k]_{\mathrm{E}}, k=1,\ldots,K\}$ of the K-D approximation, $e_{(K)}(\mathbf{x})=(P_{\mathrm{E}(K)}e)(\mathbf{x})=\sum E_k g_k(\mathbf{x})$, of the backscattered wavefield $e(\mathbf{x})$ integrated over the receiver frequency integration band F, and $P_{\mathrm{E}(K)}$ is a projector onto the K-D approximation subspace $\mathrm{E}_{(K)}=P_{\mathrm{E}(K)}\mathrm{E}=\mathrm{Span}\{g_k\}$ spanned by some chosen set of K basis functions $\{g_k(\mathbf{x})\}$. The M-by-K matrix **S** that approximates the SFO in (6) is given now by [3]

$$S_{mk}=[Sg_k,\varphi_m]_{\mathrm{U}}\ ;\quad m=1,\ldots,M\ ;\quad k=1,\ldots,K \tag{7}$$

where the set of the base functions $\{\varphi_m(\mathbf{y})\}$ that span the finite-dimensional spatial observation subspace $\mathrm{U}_{(M)}=P_{\mathrm{U}(M)}\mathrm{U}=\mathrm{Span}\{\varphi_m\}$ defines the corresponding projector $P_{\mathrm{U}(M)}$ induced by the specified array spatial response characteristics $\{\varphi_m(\mathbf{y})\}$ [1]. The vectors **E**, **N** and **U** in the EO (6) are characterized by the correlation matrices $\mathbf{R_E}=\mathbf{D}=\mathbf{D}(\mathbf{B})=\mathrm{diag}(\mathbf{B})$, $\mathbf{R_N}$, and $\mathbf{R_U}=\mathbf{S}\mathbf{R_E}\mathbf{S}^{+}+\mathbf{R_N}$, respectively, where diag(**B**) defines a diagonal matrix with vector **B** at its principal diagonal. Superscript $^{+}$ defines the adjoint operator [5] that becomes the Hermitian conjugate. The vector **B** is composed of the elements $B_k=\langle E_k E_k^{*}\rangle$; $k=1,\ldots,K$, and is referred to as a K-D vector-form approximation of the SSP. The RSS reconstruction problem is reformulated as follows: to derive an estimator for reconstructing the K-D approximations

$$\hat{\Lambda}_{(K)}(\mathbf{x})=\Lambda(\hat{B}_{(K)}(\mathbf{x}))=\Lambda(\sum_{k=1}^{K}\hat{B}_k\,|g_k(\mathbf{x})|^2)=\Lambda(\mathbf{g}^{\mathrm{T}}(\mathbf{x})\mathrm{diag}(\hat{\mathbf{B}})\mathbf{g}(\mathbf{x})) \tag{8}$$

of the relevant RSS distribution in the environment $X\ni\mathbf{x}$ via post-processing (5) whatever values of the reconstructed scene image $\hat{B}(\mathbf{x})$; $\mathbf{x}\in X$ are available. The experiment design (ED) aspects of the SSP estimation problem involving the analysis of how to choose the basis functions $\{g_k(\mathbf{x})\}$ that span the signal representation subspace $\mathrm{E}_{(K)}=P_{\mathrm{E}(K)}\mathrm{E}=\mathrm{Span}\{g_k\}$ for a given observation subspace $\mathrm{U}_{(M)}=\mathrm{Span}\{\varphi_m\}$ were investigated in more details in the previous studies [7], [16]. Here, we employ the pixel-format basis [10] and the ED considerations [1] for inducing the metrics structure in the solution space defined by the inner product

$$\|\mathbf{B}\|^2_{\mathrm{B}(K)}=[\mathbf{B},\mathbf{M}\mathbf{B}] \tag{9}$$

where **M** is referred to as the metrics inducing operator [1]. Hence, the selection of **M** provides additional geometrical degrees of freedom of the problem model. In this study, we incorporate the model of **M** that corresponds to a matrix-form approximation of the Tikhonov's stabilizer of the second order that was numerically designed in [1]. Also, following [1] we incorporate the projection-type a priori information requiring that the SSP vector **B** satisfies the linear constraint equation

$$\mathbf{G}\mathbf{B}=\mathbf{C}\ ,\quad \text{i.e. } \mathbf{G}^{-}\mathbf{G}\mathbf{B}=\mathbf{B}_P \tag{10}$$

where $\mathbf{B}_P=\mathbf{G}^{-}\mathbf{C}$ and $\mathbf{G}^{-}$ is the Moore-Penrose pseudoinverse of a given constraint operator $\mathbf{G}:\mathrm{B}_{(K)}\to\mathrm{B}_{(Q)}$, and the constraint vector $\mathbf{C}\in\mathrm{B}_{(Q)}$ and the constraint subspace $\mathrm{B}_{(Q)}(Q<K)$ are assumed to be given. In (10), the constraint operator **G** projects the

portion of the unknown SSP onto the subspace where the SSP values are fixed by **C**.

3 Generalization of the FBR Method

The estimator that produces the optimal estimate $\hat{\mathbf{B}}$ of the SSP vector via processing the M-D data recordings **U** applying the FBR estimation strategy that incorporates nontrivial a priori geometrical and projection-type model information (9), (10) was developed in our previous study [1]. Such optimal FBR estimate of the SSP is given by the nonlinear equation [1]

$$\hat{\mathbf{B}} = \mathbf{B}_P + \mathbf{P}\mathbf{B}_0 + \mathbf{W}(\hat{\mathbf{B}})(\mathbf{V}(\hat{\mathbf{B}}) - \mathbf{Z}(\hat{\mathbf{B}})) . \quad (11)$$

In (11), $\mathbf{B}_P$ is defined by (10) and $\mathbf{B}_0$ represents the a priori SSP distribution to be considered as a zero step approximation to the desires SSP $\hat{\mathbf{B}}$. In this study, we use all the notations from [1] for definitions of the sufficient statistics (SS) vector $\mathbf{V}(\hat{\mathbf{B}}) = \{\mathbf{F}(\hat{\mathbf{B}})\mathbf{U}\mathbf{U}^{+}\mathbf{F}^{+}(\hat{\mathbf{B}})\}_{\mathrm{diag}}$ ($\{\cdot\}_{\mathrm{diag}}$ defines a vector composed of the principal diagonal of the embraced matrix), the solution-dependent SS formation operator

$$\mathbf{F} = \mathbf{F}(\hat{\mathbf{B}}) = \mathbf{D}(\hat{\mathbf{B}})(\mathbf{I} + \mathbf{S}^{+}\mathbf{R}_{\mathbf{N}}^{-1}\mathbf{S}\mathbf{D}(\hat{\mathbf{B}}))^{-1}\mathbf{S}^{+}\mathbf{R}_{\mathbf{N}}^{-1} ; \quad (12)$$

the SS shift vector $\mathbf{Z}(\hat{\mathbf{B}}) = \{\mathbf{F}(\hat{\mathbf{B}})\mathbf{R}_{\mathbf{N}}\mathbf{F}^{+}(\hat{\mathbf{B}})\}_{\mathrm{diag}}$ [1], and the composite solution-dependent smoothing-projection window operator [1]

$$\mathbf{W}(\hat{\mathbf{B}}) = \mathbf{P}\boldsymbol{\Omega}(\hat{\mathbf{B}}) \quad (13)$$

with the projector

$$\mathbf{P} = (\mathbf{I} - \mathbf{G}^{-}\mathbf{G}) \quad (14)$$

and the solution-dependent regularizing window

$$\boldsymbol{\Omega}(\hat{\mathbf{B}}) = (\mathrm{diag}(\{\mathbf{S}^{+}\mathbf{F}^{+}\mathbf{F}\mathbf{S}\}_{\mathrm{diag}}) + \alpha\mathbf{D}^{2}(\hat{\mathbf{B}})\mathbf{M}(\hat{\mathbf{B}}))^{-1} , \quad (15)$$

in which the regularization parameter α is to be adaptively adjusted using the system calibration data (10). The generalization of the FBR estimator (11) for the case of RSS reconstruction in the K-D solution space can now be performed applying the mapping (8) to (11) and taking into account the pixel format of the basis $\{g_k(\mathbf{x})\}$ spanning the RSS solution space that yields

$$\hat{\Lambda}_{(K)}(\mathbf{x}) = \mathbf{g}^{\mathrm{T}}(\mathbf{x})\mathrm{diag}(\Lambda(\hat{\mathbf{B}}))\mathbf{g}(\mathbf{x}) = \sum_{k=1}^{K}\Lambda(\hat{B}_k)|g_k(\mathbf{x})|^2 ; \quad \mathbf{x} \in X . \quad (16)$$

Hence, in the adapted pixel-format solution space, the vector $\hat{\Lambda} = \boldsymbol{\Lambda}(\hat{\mathbf{B}})$ composed of pixels $\{\Lambda(\hat{B}_k); k = 1,\ldots,K\}$ represents the desired pixel-format map of the high-resolution RSS reconstruction. Because of the complexity of the solution-

dependent K-D operator inversions needed to be performed to compute the SS, $\mathbf{V}(\hat{\mathbf{B}})$, and the window, $\mathbf{W}(\hat{\mathbf{B}})$, the computational complexity of such generalized optimal algorithm (16) is extremely high. Hence, the (16) could not be addressed as a practically realizable estimator of the RSS (i.e. high-resolution RSS mapping technique realizable via performing polynomial-complex computations [12]).

4 R-FBR Technique for RSS Reconstruction

We propose the robustification scheme for quasi-real-time implementation of the generalized FBR estimator that reduces drastically the computation load of the RSS formation procedure (16) without substantial degradation in the SSP resolution and overall RSS map performances. The robust version of the FBR estimator (referred to as R-FBR method) is proposed via roughing $\mathbf{P}=\mathbf{I}$ and performing the robustification of both the SS formation operator $\mathbf{F}(\hat{\mathbf{B}})$ and the smoothing window $\mathbf{\Omega}(\hat{\mathbf{B}})$ in (11) by roughing $\mathbf{D}(\hat{\mathbf{B}})\approx\mathbf{D}=\beta\mathbf{I}$, where β represents the expected a priori image gray level [1]. Thus, the robust SS formation operator

$$\mathbf{F}=\mathbf{A}^{-1}(\rho)\mathbf{S}^{+} \quad \text{with} \quad \mathbf{A}(\rho)=\mathbf{S}^{+}\mathbf{S}+\rho^{-1}\mathbf{I} \tag{17}$$

becomes a regularized inverse of the SFO $\mathbf{S}$ with regularization parameter ρ^{-1}, the inverse of the signal-to-noise ratio (SNR) $\rho=\beta/N_0$ for the adopted white observation noise model, $\mathbf{R}_N=N_0\mathbf{I}$. The robust smoothing window

$$\mathbf{W}=\mathbf{\Omega}=(w_0\mathbf{I}+\mathbf{M})^{-1} \tag{18}$$

is completely defined now by matrix $\mathbf{M}$ that induces the metrics structure (9) in the solution space with the scaling factor $w_0=\mathrm{tr}\{\mathbf{S}^{+}\mathbf{F}^{+}\mathbf{F}\mathbf{S}\}/K$ [1]. Here, we adopt practical constraints of high SNR operational conditions [7], [9] $\rho>>1$, in which case one can neglect also the constant bias $\mathbf{Z}=Z_0\mathbf{I}$ in (11) because it does not affect the pattern of the SSP estimate. Following these practically motivated assumptions, we derive the resulting R-FBR estimator

$$\hat{\Lambda}_{RFBR}(\mathbf{x})=\mathbf{g}^{\mathrm{T}}(\mathbf{x})\mathrm{diag}(\Lambda(\mathbf{B}_0+\mathbf{\Omega}\mathbf{V}))\mathbf{g}(\mathbf{x}) \tag{19}$$

where $\mathbf{V}=\{\mathbf{F}\mathbf{U}\mathbf{U}^{+}\mathbf{F}^{+}\}_{\mathrm{diag}}$ represents now the robust (solution independent) SS vector. Thus, the principal computational load of the R-FBR estimator (19) is associated now with the operator inversions required to compute the solution operator (18) for adaptively adjusted regularization parameter ρ^{-1}. Next, the simplest rough RSS estimator can be constructed as further simplification of (19) adopting the trivial prior model information ($\mathbf{P}=\mathbf{I}$ and $\mathbf{B}_0=0\mathbf{I}$) and roughly approximation the SS formation operator $\mathbf{F}$ by the adjoint SFO, i.e. $\mathbf{F}\approx\gamma_0\mathbf{S}^{+}$ [1] (the normalizing constant γ_0 provides the balance of the operator norms, $\gamma_0^2=\mathrm{tr}^{-1}\{\mathbf{S}^{+}\mathbf{S}\mathbf{S}^{+}\mathbf{S}\}\mathrm{tr}\{\mathbf{F}\mathbf{S}\mathbf{S}^{+}\mathbf{F}^{+}\}$). In this case, the (19) is simplified to its rough version

$$\hat{\Lambda}_{MSF}(\mathbf{x})=\mathbf{g}^{\mathrm{T}}(\mathbf{x})\mathrm{diag}(\Lambda(\boldsymbol{\Omega}\mathbf{H}))\mathbf{g}(\mathbf{x}) \qquad (\mathbf{20})$$

referred to as matched spatial filtering (MSF) algorithm where the rough SS $\mathbf{H}=\gamma_0^2\{\mathbf{S}^{+}\mathbf{U}\mathbf{U}^{+}\mathbf{S}\}_{\mathrm{diag}}$ is now formed applying the adjoint operator $\mathbf{S}^{+}$, and the windowing of the rough SS is performed applying the smoothing filter $\boldsymbol{\Omega}=(w_0\mathbf{I}+\mathbf{M})^{-1}$ with nonnegative entry, the same one as was constructed numerically in [1].

5 NN for Implementing the R-FBR Method

Now, we propose a NN for efficient quasi-real-time computational implementation of the presented above R-FBR method. The main idea is to aggregate the robust regularization with the NN-based computing to reduce the computational load of the R-FBR technique. We approach this goal by performing the modifications of the multistate Hopfield-type NN originally developed in [5] and modified in [8]. Borrowing from [8] we define the Hopfield-type multistate NN as a massive interconnection of formal neurons, i.e. basic processing units. The outputs of all K neurons compose the output vector, $\mathbf{z}=\mathrm{sgn}(\mathbf{Q}\mathbf{v}+\boldsymbol{\Theta})$, where, $\mathbf{Q}$ represents the KxK matrix of the interconnection strengths of the NN, and $\boldsymbol{\Theta}$ defines the Kx1 bias vector of the NN [8]. The output vector $\mathbf{z}$ is used to update the state vector $\mathbf{v}$ of the network: $\mathbf{v}''=\mathbf{v}'+\Delta\mathbf{v}$ where, $\Delta\mathbf{v}=\Re(\mathbf{z})$ is a change of the state vector $\mathbf{v}$ computed applying the state update rule $\Re(\mathbf{z})$ and the superscripts $''$ and $'$ correspond to the state values before and after network state updating, respectively. We employ the same state update rule $\Re(\mathbf{z})$ that was designed previously in [8] that guarantees that the energy function of the overall NN

$$E_{NN}(\mathbf{v})=-\tfrac{1}{2}\mathbf{v}^{\mathrm{T}}\mathbf{Q}\mathbf{v}-\boldsymbol{\Theta}^{\mathrm{T}}\mathbf{v} \qquad (\mathbf{21})$$

is decreased at each updating step, i.e. $E_{NN}(\mathbf{v}'')\le E_{NN}(\mathbf{v}')$, until the NN reaches its stationary state related to the state $\mathbf{v}_{opt}$ at which the minimum of the NN energy (21) is attained, i.e. $E_{NN}(\mathbf{v}_{opt})=\min_{\mathbf{v}} E_{NN}(\mathbf{v})$. Next, we associate the NN's stationary state with the solution to a hypothetical inverse problem (IP) of minimization of the following composite cost function

$$E_{IP}(\mathbf{Y}|\boldsymbol{\lambda})=\tfrac{1}{2}\|\mathbf{U}-\mathbf{S}\mathbf{Y}\|^2+\tfrac{1}{2}\|\mathbf{Y}\|^2. \qquad (\mathbf{22})$$

If the regularization parameters in (22) are adjusted as $\lambda_1=1$, $\lambda_2=\rho^{-1}$ and the NN's stationary state is associated with the solution to (22) than the minimization of $E_{IP}(\mathbf{Y}|\boldsymbol{\lambda})$ provides the robust constraint least square estimate $\hat{\mathbf{Y}}=\mathbf{F}\mathbf{U}$ that uniquely defines the desired high-resolution RSS vector $\hat{\Lambda}=\Lambda(\mathbf{B}_0+\boldsymbol{\Omega}\mathbf{V})$ with SS

$\mathbf{V}=\{\hat{\mathbf{Y}}\hat{\mathbf{Y}}^{+}\}_{\text{diag}}$. Hence, the cumbersome operator inversions needed to compute the SS and reconstruct the RSS are translated now into the relevant problem of recurrent minimization of the energy function (21) of the NN and derivation of $\hat{\mathbf{Y}}=\mathbf{v}_{opt}$ via specification of the NN's parameters as follows:

$$Q_{ki}=-\lambda_1\sum_{j=1}^{K}S_{jk}S_{ji}^{*}-\lambda_2\delta_{ki}\ ;\quad \text{for all}\ \ k, I=1,\ldots,K\ . \tag{23}$$

$$\Theta_k=\lambda_1\sum_{j=1}^{K}S_{jk}U_j\ ;\qquad \text{for all}\ \ k=1,\ldots,K\ . \tag{24}$$

where Q_{ki} and Θ_k represent the elements of the interconnection strengths matrix $\mathbf{Q}$ and bias vector $\boldsymbol{\Theta}$ of the modified NN, respectively. Because of the exclusion of the solution-dependent operator inversions (17) via translations of the SS formation procedure into the relevant recurrent problem of minimization of the NN's energy function (21), the computational load of such R-FBR technique (19) is drastically decreased in comparison with the original FBR method (16).

6 Simulations

In the simulations, we considered the SAR with partially synthesized aperture as an RS imaging system [4], [13]. The SFO was factorized along two axes in the image plane: the azimuth and the range. Following the common practically motivated technical considerations [4], [9], [11] we modeled a triangular shape of the SAR range ambiguity function of 3 pixels width, and a $|sinc|^2$ shape of the side-looking SAR azimuth ambiguity function (AF) for two typical scenarios of fractionally synthesized apertures: (i) azimuth AF of 10 pixels width at the zero crossing level associated with the first system model and (ii) azimuth AF of 20 pixels width at the zero crossing level associated with the second system model, respectively. We examined the behavior and corresponding performance quality metrics of the derived above R-FBR estimator of the SSP and relevant 2-bit RSS [2], [15] for two different simulated scenes and two specified above fractional SAR models. The results of the simulation experiment indicative of the enhanced quality of SSP and RSS reconstruction with the proposed approach are reported in Figures 1 to 4 for two different RS scenes borrowed from the real-world RS imagery of the Metropolitan area of Guadalajara city, Mexico [16], [17]. Figures 1.a. thru 4.a show the original super-high resolution test scenes (not observable in the simulation experiments with partially synthesized SAR system models). Figures 1.b thru 4.b present the results of SSP imaging with the conventional MSF algorithm (20). Figures 1.c thru 4.c present the SSP reconstructed applying the proposed R-FBR method (19) implemented using the modified NN computing technique developed in the previ-

ous section. The particular reconstructed RSS reported in the simulations in Figures 1.(d,e,f) thru 4.(d,e,f) represent the so-called *hydrological electronic maps* (HEMs) [2], [15] extracted from the relevant SSP images (grouped in the corresponding upper rows of the figures) applying the weighted order statistics (WOS) classification operator $\Lambda(\hat{B}(\mathbf{x}))$ detailed in [15]. Such HEMs are specified as 2-bit hydrological RSS [2], [15] that classify the areas in the reconstructed scene images $\hat{B}(\mathbf{x})$ into four classes: areas covered with water (black zones in the figures), the high-humidity areas (dark-gray zones), the low-humidity areas (light-gray zones), and dry areas/non classified regions (white zones).

Table 1. IOSNR values provided with the R-FBR method. Results are reported for different SNRs for two test scenes and two different simulated SAR systems

SNR	First Scene				Second Scene			
[dB]	*IOSNR:* System1		*IOSNR:* System2		*IOSNR:* System1		*IOSNR:* System2	
μ	*SSP*	*HEM*	*SSP*	*HEM*	*SSP*	*HEM*	*SSP*	*HEM*
10	2.35	2.24	2.42	3.20	19.49	16.48	20.26	17.59
15	5.15	3.34	5.56	4.32	20.42	19.45	21.83	18.63
20	8.24	5.20	8.72	5.12	21.25	20.76	22.66	19.42
25	12.71	9.55	13.19	10.24	21.13	21.52	22.54	21.36

The quantitative measure of the improvement in the output signal-to-noise ratio (*IOSNR)* quality metric [4] gained with the enhanced SSP and HEM imaging methods for two simulated scenarios are reported in Table 1. All reported simulations were run for the same 512x512 pixel image format. The computation load of the enhanced RSS reconstruction with the R-FBR algorithm (19) applying the proposed above NN computational scheme in comparison with the original FBR method (16) was decreased approximately 10^5 times and required 0.38 seconds of the overall computational time for the NN-based implementation of the R-FBR technique (19) using a 2.8GHz Pentium4© computer with 512MB of memory.

7 Concluding Remarks

We have developed and presented the R-FBR method for high-resolution SSP estimation and RSS mapping as required for reconstructive RS imagery. The developed R-FBR method was implemented in a quasi-real-time mode utilizing the proposed NN computational technique. The interconnection strengths and bias inputs of the designed multistate Hopfield-type NN were specified in such a way that enabled the NN to perform the solution of the aggregated inverse problem of high-resolution SSP estimation and corresponding HEM-RSS reconstruction from the available data recordings required to implement the overall R-FBR method. The developed technique performs the balanced aggregation of the data and model prior information to perform the enhanced image reconstruction and RSS mapping

with improved spatial resolution and noise reduction. The presented simulation examples illustrate the overall imaging performance improvements gained with the proposed approach. The simulation experiment verified that the RSS extracted applying the R-FBR reconstruction method provide more accurate physical information about the content of the RS scenes in comparison with the conventional MSF and previously proposed descriptive regularization techniques [15], [16]. The presented study establishes the foundation to assist in understanding the basic theoretical and computational aspects of multi-level adaptive RS image formation, enhancement and extraction of physical scene characteristics that aggregates the robust regularization with NN-computing paradigms.

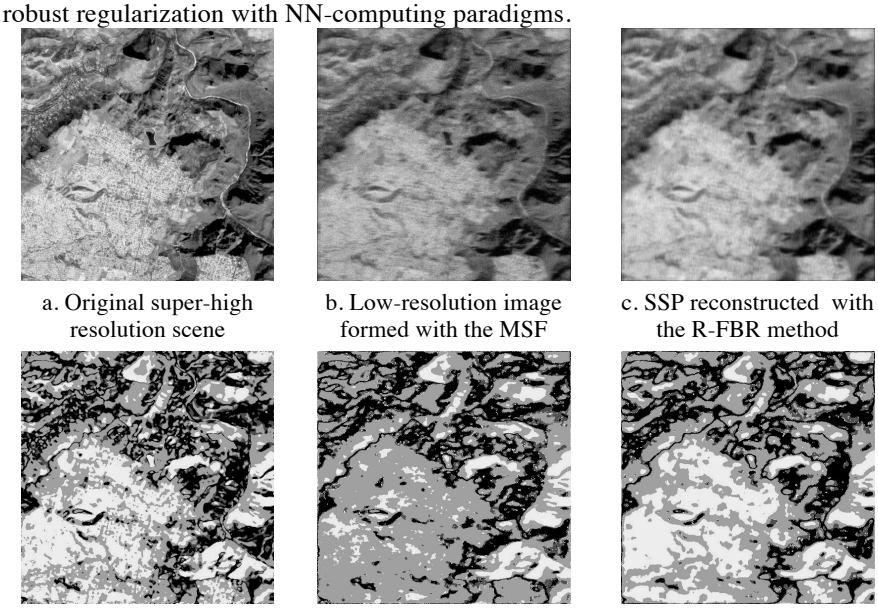

a. Original super-high resolution scene

b. Low-resolution image formed with the MSF

c. SSP reconstructed with the R-FBR method

d. HEM extracted from the original scene

e. HEM extracted from the MSF image

f. HEM extracted from the R-FBR enhanced image

Fig. 1. Simulation results for the firs scene: first system model

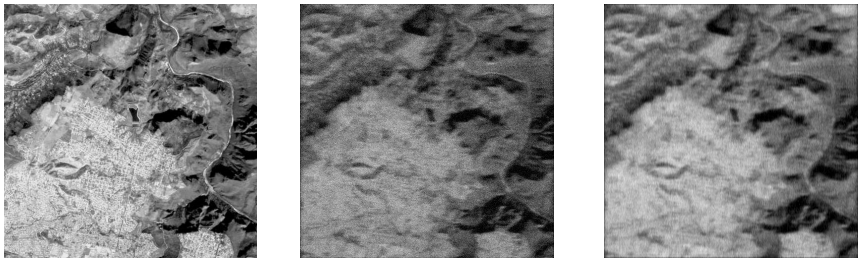

a. Original super-high resolution scene

b. Low-resolution image formed with the MSF

c. SSP reconstructed with the R-FBR method


d. HEM extracted from the original scene

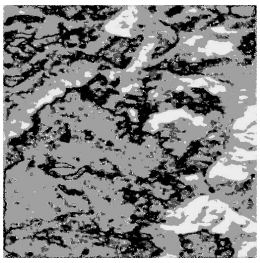
e. HEM extracted from the MSF image

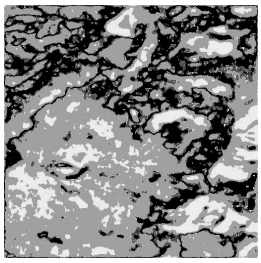
f. HEM extracted from the R-FBR enhanced image

Fig. 2. Simulation results for the firs scene: second system model

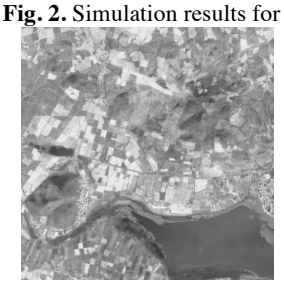
a. Original super-high resolution scene

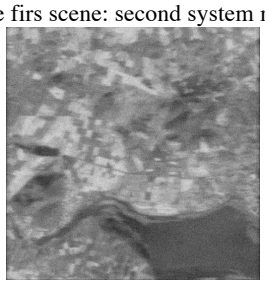
b. Low-resolution image formed with the MSF


c. SSP reconstructed with the R-FBR method

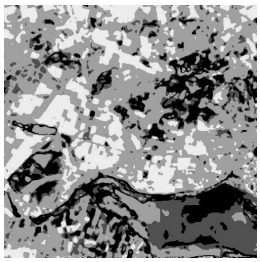
d. HEM extracted from the original scene

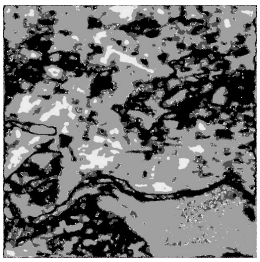
e. HEM extracted from the MSF image

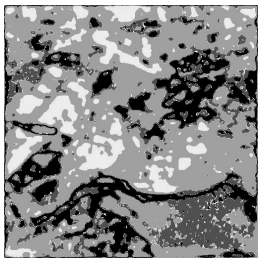
f. HEM extracted from the R-FBR enhanced image

Fig. 3. Simulation results for the second scene: first system model


a. Original super-high resolution scene

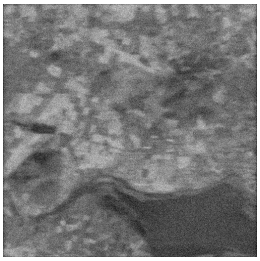
b. Low-resolution image formed with the MSF


c. SSP reconstructed with the R-FBR method

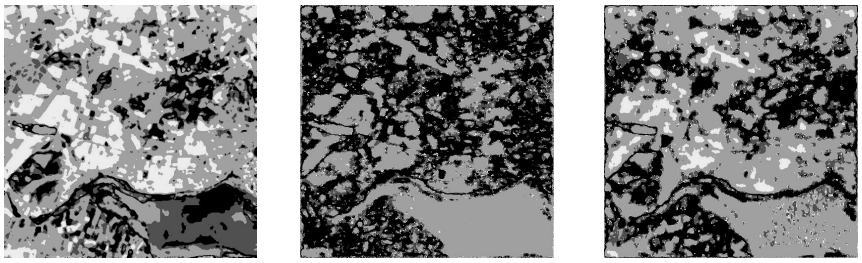

d. HEM extracted from the original scene | e. HEM extracted from the MSF image | f. HEM extracted from the R-FBR enhanced image

Fig. 4. Simulation results for the second scene: second system model

References

1. Shkvarko, Y.V.: Estimation of Wavefield Power Distribution in the Remotely Sensed Environment: Bayesian Maximum Entropy Approach. IEEE Transactions on Signal Processing. Vol. 50. IEEE, (2002) 2333-2346
2. Henderson, F.M., Lewis, A.V.: Principles and Applications of Imaging Radar. In: Manual of Remote Sensing. 3rd edn. Wiley, New York (1998)
3. Shkvarko, Y.V.: Unifying Regularization and Bayesian Estimation Methods for Enhanced Imaging with Remotely Sensed Data. Part I – Theory. IEEE Transactions on Geoscience and Remote Sensing. Vol. 42. IEEE, (2004) 923-931
4. Shkvarko, Y.V.: Unifying Regularization and Bayesian Estimation Methods for Enhanced Imaging with Remotely Sensed Data. Part II – Implementation and Performance Issues. IEEE Transactions on Geoscience and Remote Sensing. Vol. 42. IEEE, (2004) 932-940
5. Li, H.D., Kallergi, M., Qian, W., Jain, V.K., Clarke, L.P.: Neural Network with Maximum Entropy Constraint for Nuclear Medicine Image Restoration. Optical Engineering. Vol. 34. (1995) 1431-1440
6. Haykin, S.: Neural Networks: A Comprehensive Foundation. Macmillan, New York (1994)
7. Falkovich, S.E., Ponomaryov, V.I., Shkvarko, Y.V.: Optimal Reception of Space-Time Signals in Channels with Scattering. Radio I Sviaz, Moscow (1989)
8. Shkvarko, Y.V., Shmaliy, Y.S., Jaime-Rivas, R., Torres-Cisneros, M.: System Fusion in Passive Sensing using a Modified Hopfield Network. Journal of the Franklin Institute. Vol. 338. Franklin, (2001) 405-427
9. Wehner, D.R.: High-Resolution Radar. 2nd edn. Artech House, Boston (1994)
10. Barrett, H.H., Myers, K.J.: Foundations of Image Science. Wiley, New York (2004)
11. Ponomaryov, V.I., Nino-de-Rivera, L.: Order Statistics, M Method in Image and Video Sequence Processing Applications. Journal on Electromagnetic Waves and Electronic Systems. Vol. 8. Moscow (2003) 99-107
12. Starck, J.L., Murtagh, F., Bijaoui, A.: Image Processing and Data Analysis: The Multiscale Approach. Cambridge University Press, Cambridge (1998)
13. Franceschetti, G., Iodice, A., Perna, S., Riccio, D.: Efficient Simulation of Airborne SAR Raw Data of Extended Scenes. IEEE Transactions on Geoscience and Remote Sensing. Vol. 44. IEEE, (2006) 2851-2860

14. Erdogmus, D., Principe, J.C.: From Linear Adaptive Filtering to Nonlinear Information Processing. IEEE Signal Processing Magazine. Vol. 23. IEEE, (2006) 14-33
15. Perry, S.W., Wong, H.S., Guan, L.: Adaptive Image Processing: A Computational Intelligence Perspective. CRC Press, New York (2002)
16. Shkvarko, Y.V., Villalon-Turrubiates, I.E.: Dynamical Enhancement of the Large Scale Remote Sensing Imagery for Decision Support in Environmental Resource Management. In: Proceedings of the 18th Information Resource Management Association International Conference. Idea Group Inc., Vancouver (2007)
17. Space Imaging. In: http://www.spaceimaging.com/quicklook. GeoEye Inc., (2007)